blood®
Regular Article

IMMUNOBIOLOGY AND IMMUNOTHERAPY

In vivo CAR T-cell generation in nonhuman primates using lentiviral vectors displaying a multidomain fusion ligand

Christopher J. Nicolai,[1] Maura H. Parker,[1] Jim Qin,[1] Weiliang Tang,[1] Justin T. Ulrich-Lewis,[1] Rebecca J. Gottschalk,[1] Sara E. Cooper,[1] Susana A. Hernandez Lopez,[1] Don Parrilla,[1] Richard S. Mangio,[1] Nolan G. Ericson,[1] Alissa H. Brandes,[1] Saluwa Umuhoza,[1] Kathryn R. Michels,[1] Mollie M. McDonnell,[1] Lisa Y. Park,[1] Seungjin Shin,[1] Wai-Hang Leung,[1] Andrew M. Scharenberg,[1] Hans-Peter Kiem,[2] Ryan P. Larson,[1] Laurie O. Beitz,[1] and Byoung Y. Ryu[1]

[1]Umoja Biopharma, Seattle, WA; and [2]Fred Hutchinson Cancer Center, Seattle, WA

KEY POINTS

- **Lentiviral vectors displaying T-cell activation and costimulatory molecules (VivoVec) generate CAR T cells in vivo without lymphodepletion.**
- **VivoVec administration in nonhuman primates generates anti-CD20 CAR T cells in vivo, leading to prolonged complete B-cell depletion.**

Chimeric antigen receptor (CAR) T-cell therapies have demonstrated transformative efficacy in treating B-cell malignancies. However, high costs and manufacturing complexities hinder their widespread use. To overcome these hurdles, we have developed the VivoVec platform, a lentiviral vector capable of generating CAR T cells in vivo. Here, we describe the incorporation of T-cell activation and costimulatory signals onto the surface of VivoVec particles (VVPs) in the form of a multidomain fusion protein and show enhanced in vivo transduction and improved CAR T-cell antitumor functionality. Furthermore, in the absence of lymphodepleting chemotherapy, administration of VVPs into nonhuman primates resulted in the robust generation of anti-CD20 CAR T cells and the complete depletion of B cells for >10 weeks. These data validate the VivoVec platform in a translationally relevant model and support its transition into human clinical testing, offering a paradigm shift in the field of CAR T-cell therapies.

Introduction

Ex vivo–generated autologous chimeric antigen receptor T cells (CAR T cells) have exhibited remarkable efficacy in treating B-cell malignancies[1-10] and autoimmune diseases.[11-13] Despite their effectiveness, significant barriers limit their widespread use. One major hurdle is the complicated manufacturing and administration process, which requires the collection of large numbers of T cells from each individual patient, shipment of the cells to specialized manufacturing centers, ex vivo genetic engineering and expansion of the T cells into a drug product, quality control testing, and reinfusion of the CAR T-cell drug product. This process results in substantial waiting periods between initial T-cell collection and final drug product administration.[14] Lymphodepleting chemotherapy is also required to support CAR T-cell engraftment,[15] but results in significant toxicities, frequently requiring inpatient management. Collectively, the logistical complexity and cost of current CAR T-cell manufacturing and administration processes allow only a small fraction of eligible patients access to CAR T-cell therapies.[16,17]

A simpler and cost-effective alternative to current autologous CAR T-cell therapies involves the generation of CAR T cells in vivo. Recently, we described the VivoVec platform,[18] comprising third-generation, self-inactivating lentiviral particles displaying an anti-CD3 single-chain variable fragment (scFv) and pseudotyped with the low-density lipoprotein receptor–tropic cocal fusion glycoprotein (cocal is structurally similar to the vesicular stomatitis virus G fusion glycoprotein but more resistant to human serum inactivation[19,20]). The VivoVec mechanism of action involves 2 steps: (1) particle binding via the anti-CD3 scFv, resulting in T-cell activation, and the initiation of a synthetic T-cell priming program, followed by (2) cocal-mediated delivery of a CAR transgene, redirecting T-cell specificity to the CAR target. Here, we report an advance in VivoVec technology that incorporates CD80 and CD58 T-cell costimulatory ligands along with the anti-CD3 scFv to provide both T-cell activation and costimulation. We show that VivoVec particles (VVPs) incorporating CD80 and CD58 exhibit enhanced capacity for in vivo CAR T-cell generation and produce CAR T cells with increased antitumor functionality compared with those produced from VVPs

displaying anti-CD3 scFvs alone. Furthermore, we show that combining the anti-CD3 scFv together with the ligand binding domains of CD80 and CD58 into a single multidomain fusion (MDF) protein markedly augments the particles' ability to bind, activate, and transduce T cells. VVPs incorporating MDF compatible with nonhuman primate (NHP) T-cell activation and costimulation potently generate anti-CD20 CAR T cells in vivo, comprising up to 65% of circulating T cells, and result in complete B-cell depletion for up to 76 days.

Methods

Vector production

VivoVec is a third-generation lentiviral vector engineered to express MDF protein on the particles. VVPs were produced by transiently transfecting 5 plasmids (gagpol, rev, cocal, MDF, and payload) into suspension HEK 293T cells. The MDF amino acid sequence is provided in the supplemental Material (supplemental Table 3, available on the *Blood* website). After 16 hours of transfection, fresh media with 15 U/mL Denarase (c-LEcta) was added. The supernatant was harvested the next day, clarified via Mustang Q (Cytiva), filtered by tangential flow (Sartorius Vivaflow50, VF05P4), and 0.2 μm polyethersulfone sterile filtered before aliquoting and freezing.

Antibodies

All antibodies and clones listed in supplemental Tables 1 and 2.

Protein capillary immunoassay

The vector was produced and titered as previously described.[18] Particles were treated with peptide:N-glycosidase F (New England Biolabs), and 1.5 ng p24 per well was loaded into a 12-230 JESS Separation Module (Bio-Techne) as per the manufacturer's instructions. Anticocal and anti-CD3 scFv were used at 1.5 μg/mL and 20 μg/mL, respectively. Anti-CD58 and CD80 were used at 20 μg/mL and 5 μg/mL, respectively. Anti-p24 was used at 1.5 μg/mL. Secondary antibodies and chemiluminescent reagents were used per kit instructions. Data were analyzed using the Compass for SW software (Bio-Techne).

Cell lines and culture conditions

Nalm6 cells (American Type Culture Collection [ATCC]) were grown in RPMI 1640 media (Invitrogen) + 10% fetal bovine serum (Avantar) and Glutamax (Invitrogen). Human peripheral blood mononuclear cells (PBMCs) (Bloodworks) were cultured in X-VIVO 15 (Lonza) with 5% HI Human AB serum (BioIVT), 250 IU interleukin-2 (IL-2) (R&D Systems), and Glutamax (Invitrogen). For Incucyte assays, Nalm6 and LLC-MK2 cells were engineered to express NucLight near-infrared or NucLight Orange, respectively (Sartorius), and LLC-MK2 rhesus macaque cells (ATCC) were cultured in Dulbecco's modified Eagle medium (Invitrogen) + 10% fetal bovine serum + Glutamax. LLC-MK2-NLO-CD20 cells were generated via a lentivirus-encoding human CD20.

In vitro PBMC transduction

Particles were added directly to unstimulated PBMCs (human and NHP) at 2 × 10^6 cells per mL. Activation and transduction were assessed using flow cytometry on days 3 and 7, respectively. For flow cytometry, cells were stained with a fixable viability dye before surface marker staining. Data were acquired on Attune Flow Cytometers (ThermoFisher).

Particle binding

PBMCs and particles were cultured together at room temperature for 1 to 4 hours at 20 × 10^6 cells per mL at a multiplicity of infection of 2-10. Particle/T-cell binding was evaluated by flow cytometry using an anti-cocal antibody (Umoja Biopharma).

CAR T-cell killing and cytokine production

A total of 2 × 10^4 CAR^+ cells were plated with tumor cells at the indicated effector-to-target ratios in poly-D-lysine–coated plates (Corning) and cultured at 37°C and 5% CO_2. Killing was assessed by the loss of fluorescent target cells using an Incucyte (Sartorius). For serial stimulation assays, every 2 to 4 days media was removed and 4 × 10^4 Nalm6 cells were added per well. For cytokine analysis, supernatants from CAR T-cell tumor cell cultures were collected after 24 hours and measured using Meso Scale Discovery kits (Meso Scale Diagnostics).

CAR T-cell proliferation

A total of 5 × 10^4 CAR T cells were labeled with CellTrace Violet (ThermoFisher) and cultured with 5 × 10^4 Nalm6 cells in X-VIVO media lacking IL-2. Five days later, CellTrace Violet dilution was assessed on viable CAR^+ cells by flow cytometry.

PBMC-humanized mouse model

Female Nod.Cg-*Prkdc*^{scid}*IL2rg*^{tm1Wjl}/*SzJ* major histocompatibility complex (MHC) class I/II knockout (KO) mice, aged 8 to 12 weeks, (Jackson Laboratory) were used under a protocol approved by Fred Hutchinson Cancer Research Center Institutional Animal Care and Use Committee and complied with all relevant institutional and national animal welfare laws, guidelines, and policies. On day −4, mice were injected via tail vein with 2.5 × 10^5 Nalm6 cells. On day −1, mice were randomly assigned to treatment groups according to tumor burden, as measured using an in vivo imaging system (Xenogen) and humanized with 20 × 10^6 PBMCs intraperitoneally (IP). On day 0, mice received VivoVec IP at the indicated doses in a final volume of 200 μL. Tumor burden and blood collection occurred as indicated.

NHP model

The University of Washington Institutional Animal Care and Use Committee approved the protocol for this study. All pigtailed macaques (*Macaca nemestrina*) were born in domestic colonies and housed at the Washington National Primate Research Center under conditions approved by the American Association for Accreditation of Laboratory Animal Care. On day 0, animals were administered VVPs into a maximum of 4 lymph nodes (inguinal and axillary) at a maximum volume of 1 mL per node. Animals were monitored daily for temperature, activity, appetite, stool production, and general health. Blood was drawn on specific days after injection for flow analysis, DNA isolation, and clinical laboratory testing (University of Washington Clinical Laboratory). Animals exhibiting clinical and/or laboratory signs of cytokine release syndrome (CRS)/ICANS (immune cell-associated neurotoxicity syndrome) received tocilizumab (8 mg/kg IV), anakinra (10 mg/kg IV), and diazepam (1 mg/kg IV). One animal (Z20106) also received dexamethasone (4.5 mg IV × 1).

NHP transgene biodistribution

Genomic DNA was extracted from tissues using the DNeasy Blood & Tissue Kit (Qiagen). The integrated transgene was

quantified by detecting the psi packaging sequence using the QX200 AutoDG ddPCR System (Bio-Rad). Data were analyzed with QX Manager software (Bio-Rad). Primer and probe sequences are in the supplemental Table 2.

NHP RNA ISH

In situ hybridization (ISH) was performed using the RNAscope Leica System Multiplex Fluorescent Reagent Kit (Advanced Cell Diagnostics). Formalin-fixed, paraffin-embedded sections of 5 μm were heat- and protease-treated before hybridization with an RNAscope probe specific to the anti-CD20 CAR sequence. Preamplifier and amplifier were hybridized sequentially, followed by tyramide signal amplification. Cell nuclei were stained using 4′,6-diamidino-2-phenylindole (DAPI). Fluorescent images were acquired using Panoramic SCAN II digital slide scanner (3DHISTECH) under 40× magnification. Sections were analyzed by a pathologist to quantify and identify transduced cells.

Results

VVPs displaying CD80 and CD58 generate greater numbers of CAR T cells with increased in vitro and in vivo antitumor functionality

Antigen-presenting cells provide both peptide-MHC antigen presentation and costimulatory signals to T cells during priming.[21] These signals are critical to ensure proper T-cell activation, promote differentiation, gain effector functions, and form long-term memory.[22] CD28 and CD2, and their respective ligands CD80 and CD58, are key costimulatory interactions that make up the T-cell–antigen-presenting cell interface.[23-28] We hypothesized that adding CD80 and CD58 costimulatory ligands to our previous VVPs displaying anti-CD3scFv[18] would enhance their ability to activate and appropriately prime T cells, thereby generating CAR T cells with improved antitumor functionality. To test this hypothesis, VVPs were produced with or without CD80 and CD58 (supplemental Figure 1A-B), and the effect of the 2 costimulatory ligands was evaluated in in vitro cultures of PBMCs from healthy donors. Of note, unlike typical ex vivo CAR T-cell manufacturing protocols using anti-CD3/CD28 bead stimulation, VVPs are directly added to PBMCs without any exogenous stimulation. The addition of costimulatory molecules greatly enhanced the particles' ability to bind T cells (supplemental Figure 1C), leading to greater short-term T-cell activation and cytokine production (Figure 1A; supplemental Figure 1D). Although VVPs comprising anti-CD3 scFv with or without costimulatory ligands were able to generate similar percentages of CAR T cells (supplemental Figure 1E), those with costimulatory ligands led to much greater overall numbers (Figure 1B), supporting our initial hypothesis. Phenotypically, CAR T cells produced with VVPs displaying costimulatory molecules had greater surface expression of CCR7 and CD27 (supplemental Figure 1F), markers associated with memory T-cell populations and shown to positively correlate with improved clinical responses in human patients treated with ex vivo CAR T cells.[29-32] Overall, these data show that VVPs containing CD80 and CD58 costimulatory ligands exhibit increased T-cell binding and activation, leading to greater CAR T-cell generation with a less differentiated T-cell phenotype.

Next, CAR T-cell function was tested by culturing anti-CD19 CAR T cells generated with VVPs displaying costimulatory ligands or not with Nalm6 tumor cells at varying effector-to-target ratios. CAR T cells produced through the activity of VVPs displaying anti-CD3 scFv with costimulatory ligands produced similar amounts of interferon gamma but higher levels of IL-2 and tumor necrosis factor-α than the VVPs expressing anti-CD3 scFv alone (Figure 1C). CAR T cells generated by VVPs displaying costimulatory ligands also proliferated more when exposed to Nalm6 cells (supplemental Figure 1G). Furthermore, when subjected to a serial stimulation assay designed to evaluate T-cell fitness in the context of repeated antigen exposure,[33] CAR T cells generated by VVPs expressing anti-CD3 scFv with costimulatory ligands controlled tumor cell growth better over time (Figure 1D). These data demonstrate that VVPs expressing anti-CD3 scFv with costimulatory ligands generate CAR T cells with improved antitumor functionality in vitro.

In vivo antitumor efficacy was examined using a systemic Nalm6, PBMC-humanized NSG MHC I/II KO mouse model (supplemental Figure 1H), as described previously.[18] NSG MHC I/II KO mice were engrafted with Nalm6 tumor cells IV, followed by IP administration of human PBMCs. The next day, mice were treated IP with varying doses of VVPs, driving the expression of a CD19 CAR payload. Four days after VVP administration, T-cell activation was assessed by examining the expression of CD25 and CD71. Consistent with our in vitro findings, VVPs expressing an anti-CD3 scFv with costimulatory ligands induced superior T-cell activation than the VVPs with anti-CD3 scFv alone, and this occurred in a dose-dependent manner (Figure 1E). Blood CAR T-cell frequencies were evaluated 11 days after VVP administration. Consistent with the activation data, animals treated with VVPs displaying anti-CD3 scFv with costimulatory ligands demonstrated superior CAR T-cell numbers (Figure 1F-G). Finally, tumor burden was assessed over time, and animals treated with VVPs expressing anti-CD3 scFv with costimulatory ligands exhibited enhanced tumor control at lower doses (Figure 1H). Overall, these data indicate that VVPs comprising anti-CD3 scFv together with costimulatory ligands generate CAR T cells in vivo that exhibit greater antitumor efficacy relative to CAR T cells generated by VVPs comprising anti-CD3 scFv alone in a humanized mouse leukemia model.

An MDF protein comprising costimulatory molecules enhances T-cell activation and transduction

We designed an MDF protein consisting of CD58, the anti-CD3 scFv, and CD80 in a single polypeptide (supplemental Figure 2A) to simplify VVP manufacturing and showed successful packaging of the MDF protein on VVPs (supplemental Figure 1A). Unexpectedly, VVPs displaying the MDF protein (referred here as MDF VVPs) exhibited much greater binding to T cells than to the particles containing the individual costimulatory molecules with a separate anti-CD3 scFv (Figure 2A) and resulted in higher T-cell CD25 expression (Figure 2B), without eliciting increases in particle-induced cytokine production (supplemental Figure 2B). Remarkably, MDF VVPs generated CAR T cells much more efficiently in vitro, particularly at low multiplicity of infection (Figure 2C). CAR T cells generated with MDF VVPs had comparable surface expression of CCR7 and CD27 memory cell markers (supplemental Figure 2C), suggesting that the quality of CAR T cells is comparable to VVPs with individually displayed costimulatory

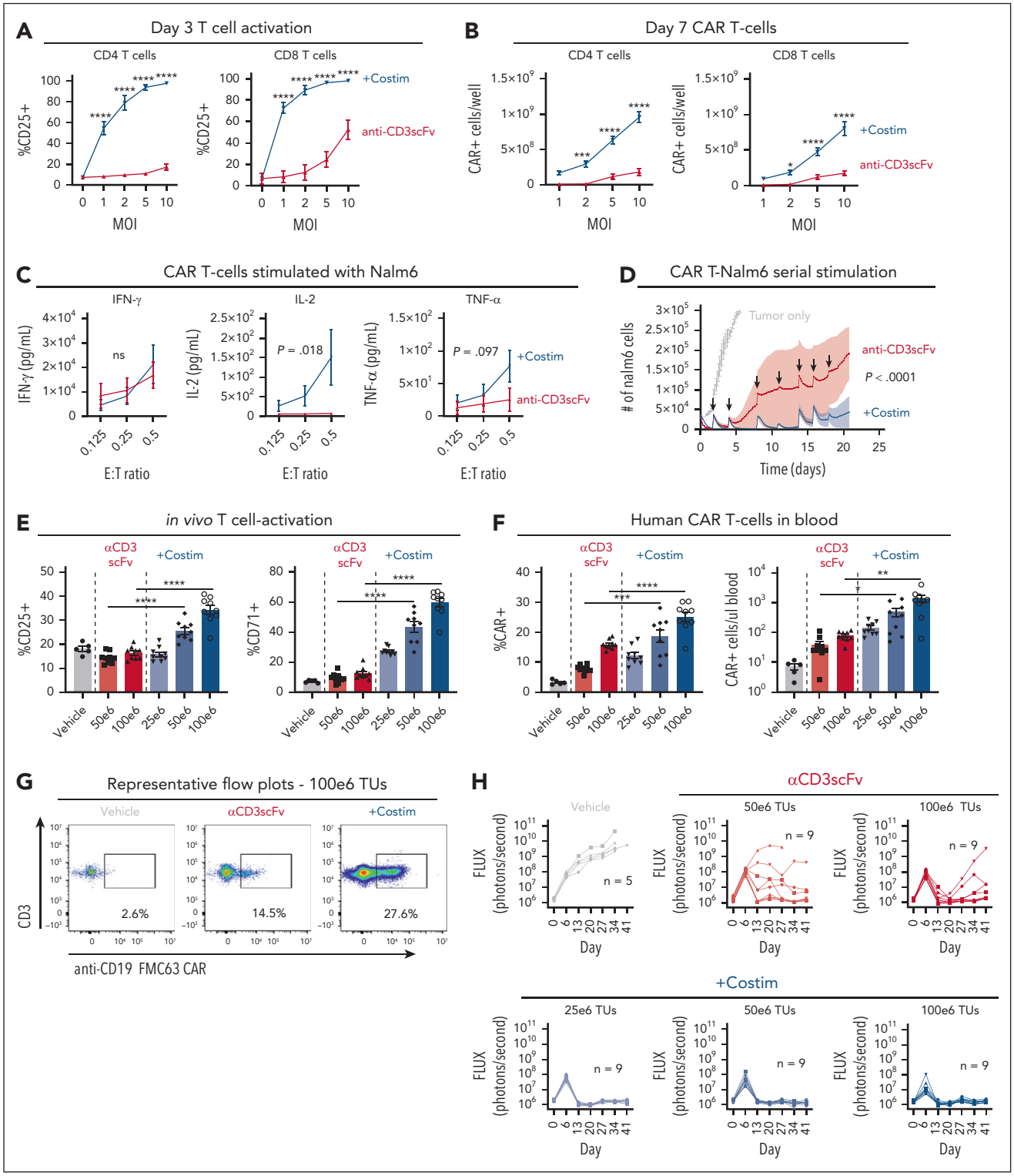

Figure 1. VVPs containing CD80 and CD58 costimulatory domains enhance T-cell activation and generate greater numbers of CAR T cells with increased in vitro and in vivo antitumor functionality. (A) VivoVec–induced CD4 and CD8 T-cell activation, as measured by CD25, 3 days after VVP addition, n = 3 PBMC donors and representative of 5 individual experiments. (B) Total CAR$^+$ CD4 and CD8 T cells generated by VVPs in vitro, 7 days after vector addition. Data combined from 2 separate experiments with n = 3 PBMC donors for each. (C) CAR T-cell cytokine production (interferon gamma [IFN-γ], IL-2, and tumor necrosis factor-α [TNF-α]) upon Nalm6 coculture for 24 hours. Representative of 2 individual experiments, n = 3 PBMC donors. (D) CAR T-cell–Nalm6 in vitro serial stimulation assay, representative of 2 individual experiments, n = 3 PBMC donors. Arrows indicate restimulation with fresh Nalm6 cells. (E) Human T-cell activation, as measured by CD25 and CD71, in humanized NSG MHC I/II KO model 4 days after VivoVec administration at several particle doses, n = 5 to 9. (F) Percentage of CD19 CAR$^+$ of human CD3$^+$ cells and total human CD19 CAR$^+$ cells per μL blood at day 11 after VivoVec particle administration, n = 5 to 9. (G) Representative flow plots for panel F. (H) Tumor burden over time as measured by Nalm6 bioluminescence, n = 5 to 9. Two-way analysis of variance (ANOVA) with Sidak multiple comparisons for panels A-B. Two-way ANOVA for panels C-D. Two-tailed unpaired student *t* test for panels E-F. ****P < .0001; ***P < .0002; **P < .002; and *P < .03. +Costim, VVP displaying anti-CD3scFv, CD80, and CD58 costimulatory ligands; MOI, multiplicity of infection; ns, not significant; TU, transducing units.

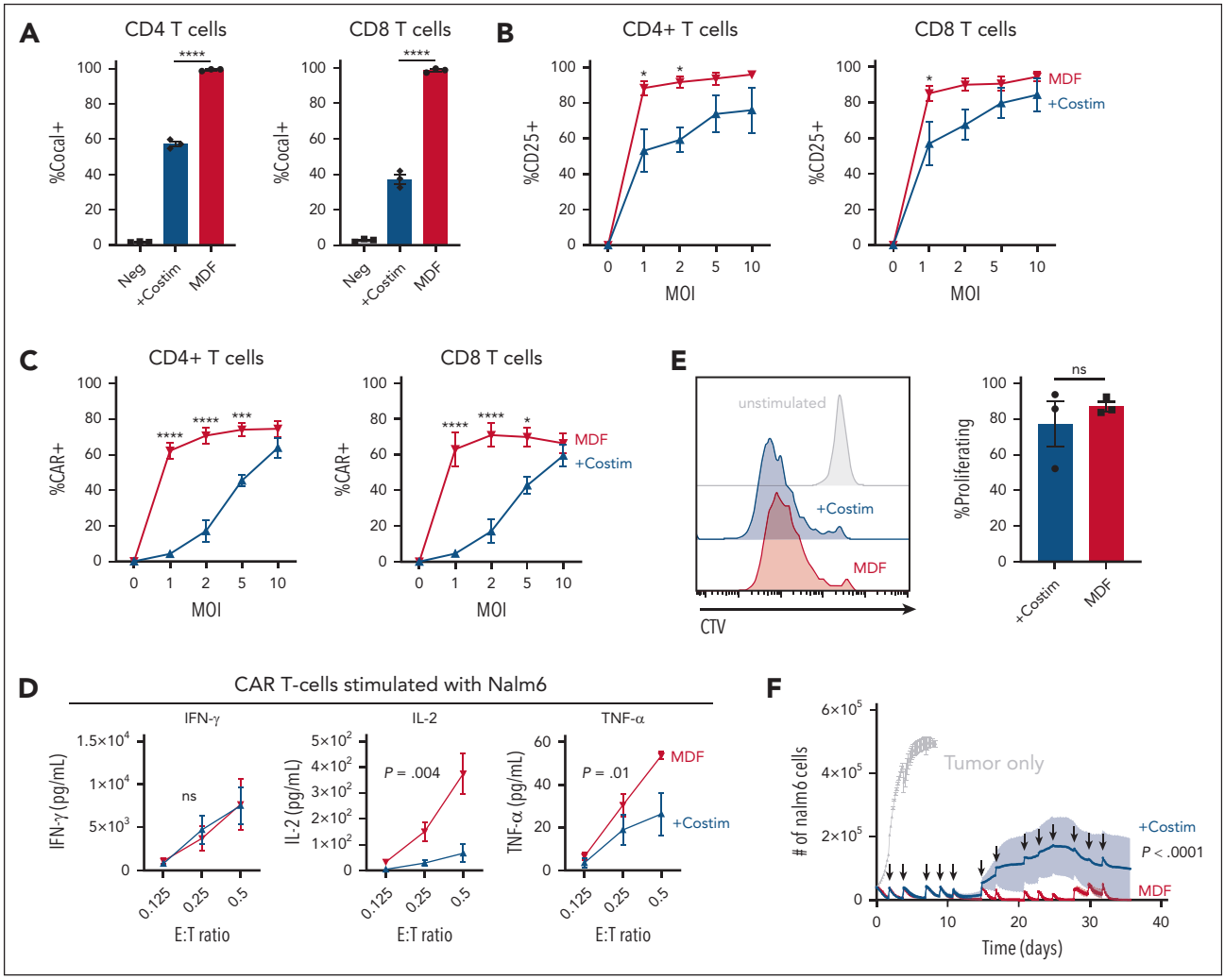

Figure 2. MDF protein comprising an anti-CD3 scFv fused to the CD58 extracellular domain and CD80 exhibit potentiated T-cell activation and transduction-enhancing properties. (A) VivoVec T-cell–binding assay. A total of 20 × 10^6 PBMCs cultured with VivoVec at MOI = 10 for 1 hour followed by flow cytometry for T-cell–associated cocal glycoprotein, n = 3 PBMC donors and representative of 2 individual experiments. (B) VivoVec–induced CD4 and CD8 T-cell activation, as measured by CD25, 3 days after vector addition, n = 3 PBMC donors and representative of 3 individual experiments. (C) Percent of CD4 and CD8 T cells expressing anti-CD19 CAR 7 days after VivoVec addition to PBMCs, n = 3 PBMC donors and representative of 3 individual experiments. (D) CAR T-cell cytokine production (IFN-γ, IL-2, and TNF-α) upon Nalm6 coculture for 24 hours, representative of 2 individual experiments, n = 3 PBMC donors. (E) CellTrace Violet (CTV) dilution on VivoVec–generated anti-CD19 CAR T cells 5 days after Nalm6 stimulation, representative of 2 independent experiments, n = 3 PBMC donors. (F) CAR T-cell–Nalm6 in vitro serial stimulation assay, representative of 2 individual experiments, n = 3 PBMC donors. Arrows indicate restimulation with fresh Nalm6 cells. Two-tailed unpaired student *t* test for panels A,E. Two-way ANOVA with Sidak multiple comparisons for panels B-C. Two-way ANOVA for panels D,F. ****$P < .0001$; ***$P < .0002$; and *$P < .03$.

molecules. In support of this, MDF VVP–generated anti-CD19 CAR T cells produced similar amounts of interferon gamma and proliferated similarly when cocultured with Nalm6 cells (Figure 2D-E). Interestingly, MDF VVP–generated CAR T cells produced more IL-2 and tumor necrosis factor-α upon Nalm6 coculture (Figure 2D), suggesting that MDF VVP–generated CAR T cells may be more functional.[34] Consistent with enhanced antitumor function and persistence, MDF VVP–generated CAR T cells were better able to control Nalm6 tumor growth in a serial stimulation assay (Figure 2F) and even outperformed CAR T cells generated using conventional αCD3/αCD28 (Dynabeads)–based stimulation protocols (supplemental Figure 2D). These data show that MDF VVPs generate CAR T cells more efficiently in vitro with enhanced antitumor functionality.

MDF VVPs exhibit enhanced in vivo functionality in a humanized mouse leukemia model

We next examined MDF VVP antitumor function in vivo using the NSG MHC I/II KO mouse model described above. Consistent with in vitro observations, MDF VVPs demonstrated increased potency in the context of activating T cells in the blood compared with VVPs displaying anti-CD3 scFv and individual costimulatory ligands (Figure 3A). On day 11, we observed that both particles generated similar percentages of CAR T cells in blood, but MDF-containing particles led to greater overall numbers (Figure 3B). This is likely due to increased general T-cell activation and subsequent proliferation induced by the MDF protein. Fewer CAR T cells were observed in the blood than in the previous in vivo xenograft experiment (Figure 1). These types of differences between in vivo xenograft

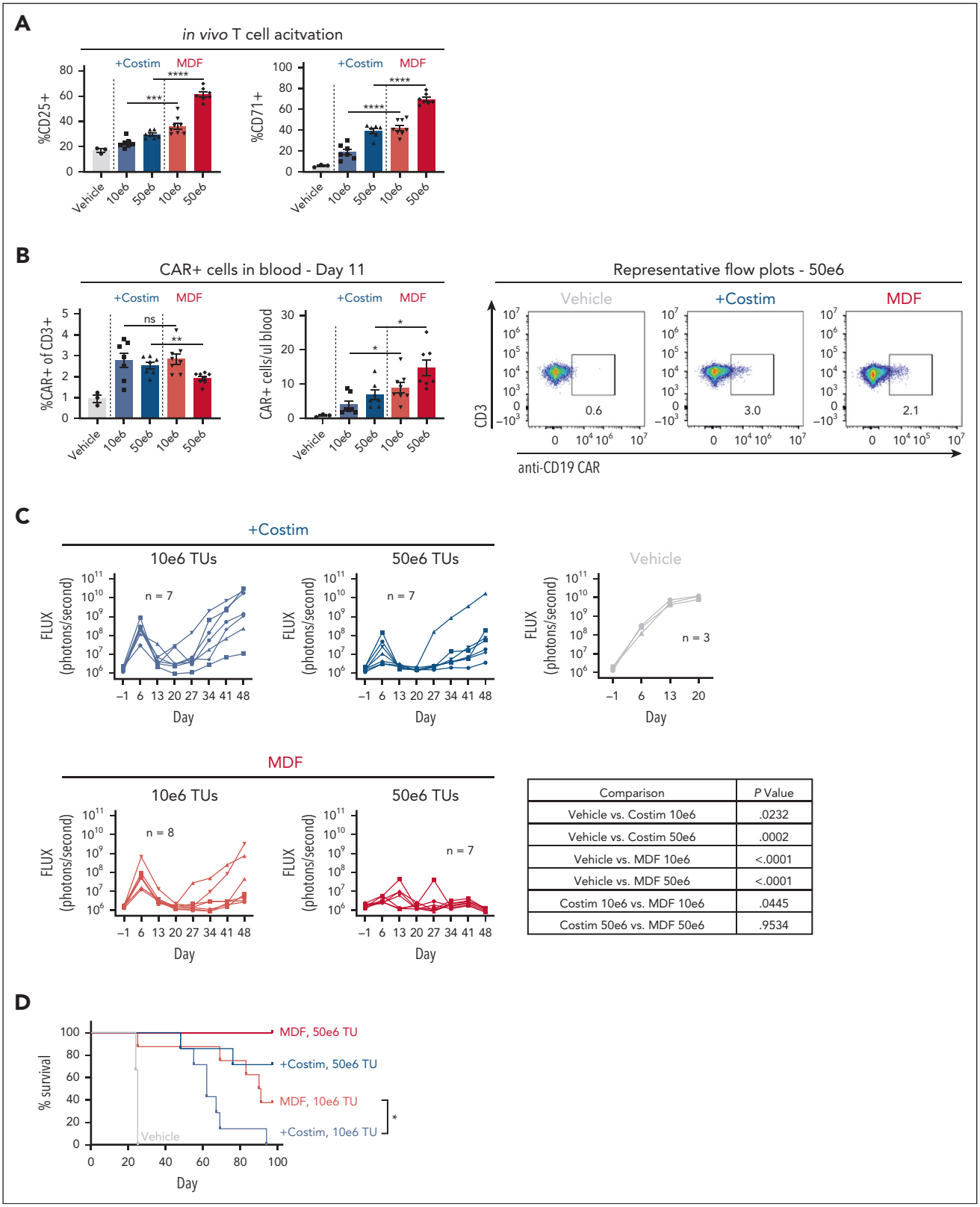

Comparison	*P* Value
Vehicle vs. Costim 10e6	.0232
Vehicle vs. Costim 50e6	.0002
Vehicle vs. MDF 10e6	<.0001
Vehicle vs. MDF 50e6	<.0001
Costim 10e6 vs. MDF 10e6	.0445
Costim 50e6 vs. MDF 50e6	.9534

Figure 3. MDF VVPs exhibit enhanced in vivo functionality in a humanized NSG MHC I/II KO Nalm6 mouse model. (A) Human T-cell activation, as measured by CD25 and CD71, in humanized NSG MHC I/II KO model 4 days after VivoVec administration. (B) Percent CD19 CAR$^+$ of human CD3$^+$ cells and total human CD19 CAR$^+$ cells per microliter blood (left) and representative flow plots (right) on day 11 after VivoVec administration. (C) Tumor burden over time as measured by Nalm6 bioluminescence. (D) Overall survival. For all figures, n = 7 to 8 for VivoVec groups and n = 3 for vehicle control. Two-tailed unpaired student *t* test for panels A-B. Two-way ANOVA with multiple comparisons for panel C. Log-rank Mantel Cox test for panel D. ****P < .0001; ***P < .0002; **P < .002; and *P < .03.

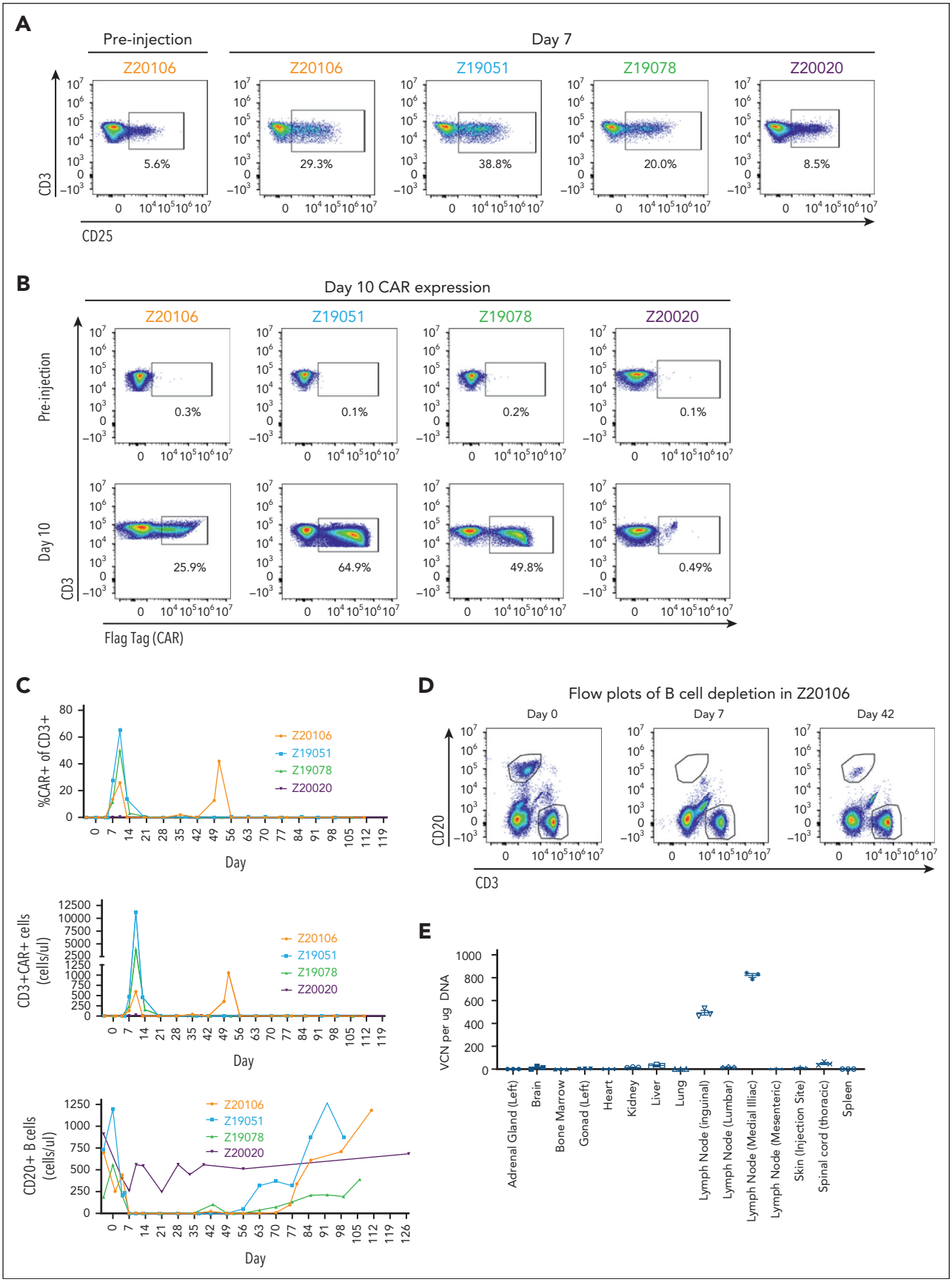

Figure 4.

experiments are commonly observed and are caused by donor variation in T-cell responses in these models. Tumor burden was measured over time using bioluminescent Nalm6 tumor cells. Although both types of particles were able to elicit tumor control, MDF VVPs performed slightly better in primary tumor clearance and in overall survival (Figure 3C-D). This was especially evident at the lower dose of 10×10^6 transducing units, where the median survival of animals treated with MDF VVPs was 90.5 days, compared with 62 days for the individual costimulatory molecule particles (Figure 3D). Notably, at the higher dose of 50×10^6 transducing units, MDF VVP-treated animals achieved 100% survival for the duration of the study (Figure 3D). Taken together, these data demonstrate that VVPs displaying the MDF protein have superior antitumor efficacy relative to VVPs expressing an anti-CD3 scFv and individual costimulatory ligands in a humanized mouse leukemia model.

MDF VVPs administered intranodally induce potent and prolonged B-cell depletion in NHPs

Although informative, humanized mouse models have limitations and do not recapitulate the full extent of an animal's immune system, notably a complete lack of normally developed secondary lymphoid tissue and susceptibility to xenogeneic graft-vs-host disease.[35] To address these limitations, we developed an NHP model in *M nemestrina* because of this species' permissiveness to transduction with HIV-1–derived lentiviral vectors.[36] For this model, we used a NHP/human cross-reactive anti-CD20 CAR previously shown to deplete B cells using ex vivo–manufactured CAR T cells in rhesus macaques.[37] To make the MDF protein suitable for this model, we substituted an anti-NHP CD3 scFv[38] for the anti-human CD3 scFv. Human CD58 and CD80 were retained because of the high sequence homology of these proteins between both species (supplemental Figure 3A).

NHP surrogate MDF VVPs were validated in vitro by assessing their binding, activation, and transduction of *M nemestrina* CD4 and CD8 T cells (supplemental Figure 3B) and the resultant CAR T-cell cytolytic function through killing assays targeting CD20-expressing NHP LLC-MK2 cells (supplemental Figure 3C). Collectively, these results indicate that surrogate NHP MDF VVPs bind, activate, and transduce NHP T cells with comparable potency to human MDF VVPs.

Supplemental Figure 3D details the in vivo experimental protocol in our NHP model. Briefly, NHP MDF VVPs carrying an anti-CD20 CAR payload were administered at varying doses into the lymphatic vasculature of 4 animals via lymph node injection. The intranodal route of administration was chosen to enable efficient particle T-cell interaction while reducing systemic tissue exposure to free particles compared with the intravenous route. Animals were bled 1 to 2 times per week to assess particle-induced T-cell activation, CAR expression, and subsequent B-cell depletion by flow cytometry. Animals were also monitored for signs of CRS and ICANS. Importantly, neither lymphodepletion nor exogenous cytokine supplementation was used in our study.

Three of 4 animals demonstrated NHP MDF VVP–induced T-cell activation 7 days after particle administration (Figure 4A). Among these 3 animals, NHP MDF VVP administration was remarkably potent, generating populations of CAR T cells comprising as many as 65% of circulating T cells at day 10 (Figure 4B), corresponding to 596, 3875, and 11 182 CAR T cells per microliter of blood (Figure 4C). As expected, the appearance of CAR T cells in circulation coincided with the loss of B cells, and by day 7, circulating B cells were undetectable in all animals with detectable CAR T cells (Figure 4C-D). As part of a dose de-escalation study, 1 animal (Z20020) received a fivefold lower dose of VVPs (supplemental Figure 3D). We did not observe obvious signs of T-cell activation (Figure 4A), meaningful levels of CAR expression (Figure 4B), or evidence of complete B-cell depletion (Figure 4C) in this animal. In contrast, in the 3 animals that generated CAR T cells, loss of circulating B cells was both consistent and unexpectedly durable, with circulating B cells largely undetectable through 56, 63, and 76 days of treatment. Notably, 1 animal (Z20106) demonstrated a large re-expansion of blood CAR T cells at day 49 in response to the reappearance of a small population of B cells evident on study day 42 (Figure 4D). This suggests that VivoVec generated CAR T cells with prolonged persistence, which could indicate generation of memory CAR T cells. Consistent with memory T-cell formation, B cells also reappeared in the circulation of a second animal (Z19078) at day 43, followed by loss again by day 49. B cells remained undetectable in this animal up until day 63, suggesting persistent and ongoing antigen-specific memory CAR T-cell function (Figure 4D).

In terms of CRS, we observed elevated C-reactive protein (CRP) levels shortly before CAR T cells were detected in the blood (supplemental Figure 3E), suggesting that these events are CAR T-cell–mediated rather than particle-driven. This was short-lived, with CRP levels normalizing as CAR T cells disappeared from the blood by day 14. As described above, 1 animal experienced a resurgence in blood CAR T cells at day 49 (Figure 4C), again associated with another short-lived elevation in CRP (supplemental Figure 3E). IL-6 was also elevated shortly before CAR T cells were observed in the blood, normalizing with CAR T-cell retraction. Like CRP, the animal that experienced a resurgence in blood CAR T cells also had elevated IL-6 during this time. Ferritin and temperature followed a similar pattern, with increases correlating with initial CAR T-cell detection in the blood and at later time points when CAR T cells were detected (supplemental Figure 3E). In addition to CRS symptoms, we observed mild tremors and brief seizure activity in the first 2 animals treated. These events were short-lived and coincided with peak CAR T-cell expansion observed at day 10. In response, tocilazumab and anakinra were administered, and the tremors resolved. We did not observe any overt signs of liver toxicity, with alanine transaminase, aspartate aminotransferase, and alkaline

Figure 4. MDF VVPs administered intranodally induce potent and prolonged B-cell depletion in NHPs. (A) Activation of NHP T cells in the blood 7 days after VivoVec administration, as measured by CD25. (B) Anti-CD20 CAR expression (Flag-tag) on NHP $CD3^+$ T cells in the blood 10 days after VivoVec administration. (C) Percent of NHP T cells expressing CAR (top), overall numbers of CAR positive T cells (middle), and total B cells in the blood (bottom) over time. (D) Representative flow plots of B-cell depletion in Z20106. (E) Biodistribution of VivoVec CAR payload in various tissues 139 days after particle administration in Z20106, measured by ddPCR. VCN, vector copy number.

phosphatase remaining within the normal range, except for a brief mild elevation in alanine transaminase and aspartate aminotransferase on day 1 in 1 animal only (supplemental Figure 3F).

Finally, to assess the biodistribution of transduced cells, 1 animal with the longest post-VVP treatment period (139 days) was taken to necropsy, and 20 different tissues were assessed for vector genome integration by droplet digital polymerase chain reaction (ddPCR). The anti-CD20 CAR transgene was clearly detectable in genomic DNA sourced from the injected inguinal lymph node and in the immediately downstream medial iliac lymph node (Figure 4E). We were unable to detect significant levels of CAR transgene from the genomic DNA extracted from any of the other tissues analyzed, suggesting that cells containing transgenes in DNA form are primarily sequestered in the injected and adjacent lymph nodes for several months after VivoVec treatment. In an orthogonal method, we also examined biodistribution by RNA ISH targeting the CAR transgene. Consistent with the ddPCR data, we were able to detect CAR expression in a very small number of cells in the injected inguinal lymph node and downstream medial iliac node (supplemental Figure 3G). We also detected low-level signals in the spleen, bone marrow, and lung, which we believe are indicative of CAR^+ cells trafficking to these locations. We did not detect the CAR payload in any other tissues examined, consistent with the ddPCR data. Overall, these data show that VivoVec, delivered via intralymphatic injection, efficiently generates CAR T cells in an immunocompetent NHP in the absence of lymphodepletion. The CAR T cells were highly functional, leading to B-cell aplasia for up to 76 days.

Discussion

Adoptive cell therapies with autologous ex vivo–manufactured CAR T cells are a clinically validated therapeutic approach for B-cell malignancies, but challenges associated with manufacturing and administration prevent their widespread use. We previously demonstrated in vivo CAR T-cell generation using VivoVec, a novel T-cell–engineering platform capable of generating in vivo CAR T cells without lymphodepleting chemotherapy.[18] Here, we describe significant improvements made to the VivoVec platform by incorporating CD80 and CD58 costimulatory molecules in the form of a MDF protein on the surface of VVPs and validate the feasibility of in vivo CAR T therapy in NHPs. The MDF VVPs were remarkably potent, generating large numbers of peripheral CAR T cells and sustaining B-cell depletion for over 10 weeks after a single dose and in the absence of lymphodepleting chemotherapy. These results are striking when compared with a benchmark study in rhesus macaques using ex vivo–manufactured anti-CD20 CAR T cells with lymphodepleting chemotherapy, in which B cells were observed to rebound 32 and 43 days after treatment.[37] We also saw evidence of CAR T-cell memory responses, with 1 animal displaying a resurgence of peripheral CAR T cells 49 days after treatment, reflecting a persistent CAR T-cell population that re-expanded in response to a small increase in circulating B cells. In a second animal, we observed a re-emergence in circulating B cells at day 43, which was cleared by day 49. Although circulating CAR T cells remained low in this animal, the absence of B cells requires ongoing CAR T-cell activity, supporting the existence of a memory response.

Alternative approaches to enable cell-selective in vivo T-cell transduction have previously been described.[39-45] MDF VivoVec differentiates itself through the engagement of both the T-cell receptor complex and costimulatory molecules upon T-cell binding. By doing so, VVPs replicate physiologically critical priming signals, generating abundant, high-quality CAR T cells that expand in a similar manner to endogenous T cells responding to their cognate antigen.[22] This may explain why we readily detected CAR T cells by flow cytometry in the blood of NHPs, whereas alternative in vivo delivery approaches, which lack costimulation, have thus far been unable to do so.[46,47]

VivoVec uses the cocal glycoprotein for cell entry via the low-density lipoprotein receptor[48] and presents a hypothetical risk for off-target transduction due to the receptor's broad expression. In a single animal biodistribution study, we detected integrated transgenes by ddPCR solely in the injected inguinal node and the downstream medial iliac lymph node 139 days after treatment. The detection of signals in these nodes is expected given the lymph node route of administration. By RNA ISH, we detected rare (<1%) transgene signals in the spleen, bone marrow, and lung. These are common sites of lymphocyte trafficking, and the detection of low-level signals is likely accounted for by the trafficking of previously transduced lymphocytes or myeloid cells. Importantly, we did not observe evidence of off-tissue transduction in hepatocytes, which were previously reported to be a site of vesicular stomatitis virus G–pseudotyped lentiviral biodistribution.[49,50] We speculate that the binding specificity of MDF VVPs to T cells substantially limits the particles' contact with non-T cells and that lymph node injection maximizes the time for particle T-cell contact and stable binding to occur, thus limiting the systemic distribution of free particles. Collectively, these factors enable VivoVec to achieve both efficient and highly specific in vivo gene delivery to T cells.

Autologous CAR T-cell therapies have demonstrated remarkable efficacy in the treatment of B-cell malignancies, but significant challenges in their manufacturing and administration hinder their widespread use. In vivo generation of CAR T cells is an emerging methodology and may alleviate these significant logistical issues. Our study provides a clear proof-of-principle for the VivoVec platform and demonstrates efficient in vivo generation of highly functional CAR T cells in NHPs. These results position VivoVec–based drug products for transition to human clinical studies, with the potential for substantially expanding patient access to transformational CAR T-cell therapies across oncology and autoimmune disease indications.

Acknowledgments

The authors thank Audrey Germond, Marbella Magana, William Garrison, Melissa Berg, Alex Christodoulou, Joel Ahrens, Jesse Day, Charlotte Hotchkiss, Chris English, Audrey Baldessari, and the rest of the staff at the Washington National Primate Research Center for expert assistance with the nonhuman primate studies. The authors also thank Katie Merriman for helpful comments and assistance with intellectual property filings.

This work was funded by Umoja Biopharma, a clinical-stage for-profit biotechnology company.

Authorship

Contribution: C.J.N., M.H.P., J.Q., J.T.U.-L., R.J.G., S.E.C., S.A.H.L., D.P., R.S.M., N.G.E., A.H.B., S.U., K.R.M., and L.Y.P. performed and analyzed experiments; C.J.N., W.T., M.M.M., and S.S. contributed vital reagents; C.J.N., M.H.P., W.-H.L., A.M.S., H.-P.K., R.P.L., L.O.B., and B.Y.R. conceived of the study, provided critical feedback, and helped shape the research and analysis; C.J.N., A.M.S., L.O.B., and B.Y.R. wrote the manuscript; and all authors critically read the manuscript.

Conflict-of-interest disclosure: All authors, except for H.-P.K., are paid employees of Umoja Biopharma and hold equity in the company. H.-P.K. is a member of the scientific advisory board at Umoja Biopharma.

ORCID profiles: C.J.N., 0000-0001-9838-1419; K.R.M., 0000-0002-8227-8238; M.M.M., 0000-0002-6984-3562; L.Y.P., 0009-0004-8213-3516; H.-P.K., 0000-0001-5949-4947.

Correspondence: Laurie O. Beitz, Umoja Biopharma, 1150 Eastlake Ave E, Suite 400, Seattle, WA 98109; email: laurie.beitz@umoja-biopharma.com; and Byoung Y. Ryu, Umoja Biopharma, 1150 Eastlake Ave E, Suite 400, Seattle, WA 98109; email: byoung.ryu@umoja-biopharma.com.

Footnotes

Submitted 5 March 2024; accepted 31 May 2024; prepublished online on *Blood* First Edition 11 June 2024. https://doi.org/10.1182/blood.2024024523.

Data are available on request from the corresponding authors, Laurie O. Beitz (laurie.beitz@umoja-biopharma.com) and Byoung Y. Ryu (byoung.ryu@umoja-biopharma.com).

The online version of this article contains a data supplement.

There is a *Blood* Commentary on this article in this issue.

The publication costs of this article were defrayed in part by page charge payment. Therefore, and solely to indicate this fact, this article is hereby marked "advertisement" in accordance with 18 USC section 1734.

REFERENCES

1. Neelapu SS, Locke FL, Bartlett NL, et al. Axicabtagene ciloleucel CAR T-cell therapy in refractory large B-cell lymphoma. *N Engl J Med*. 2017;377(26):2531-2544.
2. Maude SL, Laetsch TW, Buechner J, et al. Tisagenlecleucel in children and young adults with B-cell lymphoblastic leukemia. *N Engl J Med*. 2018;378(5):439-448.
3. Schuster SJ, Svoboda J, Chong EA, et al. Chimeric antigen receptor T cells in refractory B-cell lymphomas. *N Engl J Med*. 2017;377(26):2545-2554.
4. Zhao W-H, Wang B-Y, Chen L-J, et al. Four-year follow-up of LCAR-B38M in relapsed or refractory multiple myeloma: a phase 1, single-arm, open-label, multicenter study in China (LEGEND-2). *J Hematol Oncol*. 2022;15(1):86.
5. Schmidts A, Ormhøj M, Choi BD, et al. Rational design of a trimeric APRIL-based CAR-binding domain enables efficient targeting of multiple myeloma. *Blood Adv*. 2019;3(21):3248-3260.
6. Brentjens RJ, Davila ML, Riviere I, et al. CD19-targeted T cells rapidly induce molecular remissions in adults with chemotherapy-refractory acute lymphoblastic leukemia. *Sci Transl Med*. 2013;5(177):177ra38.
7. Kochenderfer JN, Rosenberg SA. Treating B-cell cancer with T cells expressing anti-CD19 chimeric antigen receptors. *Nat Rev Clin Oncol*. 2013;10(5):267-276.
8. Gardner RA, Finney O, Annesley C, et al. Intent-to-treat leukemia remission by CD19 CAR T cells of defined formulation and dose in children and young adults. *Blood*. 2017;129(25):3322-3331.
9. Raje N, Berdeja J, Lin Y, et al. Anti-BCMA CAR T-cell therapy bb2121 in relapsed or refractory multiple myeloma. *N Engl J Med*. 2019;380(18):1726-1737.
10. Brudno JN, Maric I, Hartman SD, et al. T cells genetically modified to express an anti-B-cell maturation antigen chimeric antigen receptor cause remissions of poor-prognosis relapsed multiple myeloma. *J Clin Oncol*. 2018;36(22):2267-2280.
11. Mackensen A, Müller F, Mougiakakos D, et al. Anti-CD19 CAR T cell therapy for refractory systemic lupus erythematosus. *Nat Med*. 2022;28(10):2124-2132.
12. Müller F, Boeltz S, Knitza J, et al. CD19-targeted CAR T cells in refractory antisynthetase syndrome. *Lancet Lond Engl*. 2023;401(10379):815-818.
13. Bergmann C, Müller F, Distler JHW, et al. Treatment of a patient with severe systemic sclerosis (SSc) using CD19-targeted CAR T cells. *Ann Rheum Dis*. 2023;82(8):1117-1120.
14. Mikhael J, Fowler J, Shah N. Chimeric antigen receptor T-cell therapies: barriers and solutions to access. *JCO Oncol Pract*. 2022;18(12):800-807.
15. Kansagra AJ, Frey NV, Bar M, et al. Clinical utilization of chimeric antigen receptor T-cells (CAR-T) in B-cell acute lymphoblastic leukemia (ALL)-an expert opinion from the European Society for Blood and Marrow Transplantation (EBMT) and the American Society for Blood and Marrow Transplantation (ASBMT). *Bone Marrow Transplant*. 2019;54(11):1868-1880.
16. Puckrin R, Stewart DA, Shafey M. Real-world eligibility for second-line CAR-T cell therapy in large B-cell lymphoma: a population-based analysis. *Transplant Cell Ther*. 2022;28(4):218.e1-218.e4.
17. Hernandez I, Prasad V, Gellad WF. Total costs of chimeric antigen receptor T-cell immunotherapy. *JAMA Oncol*. 2018;4(7):994-996.
18. Michels KR, Sheih A, Hernandez SA, et al. Preclinical proof of concept for VivoVec, a lentiviral-based platform for in vivo CAR T-cell engineering. *J Immunother Cancer*. 2023;11(3):e006292.
19. Trobridge GD, Wu RA, Hansen M, et al. Cocal-pseudotyped lentiviral vectors resist inactivation by human serum and efficiently transduce primate hematopoietic repopulating cells. *Mol Ther*. 2010;18(4):725-733.
20. Rajawat YS, Humbert O, Cook SM, et al. In vivo gene therapy for canine SCID-X1 using cocal-pseudotyped lentiviral vector. *Hum Gene Ther*. 2021;32(1-2):113-127.
21. Cabeza-Cabrerizo M, Cardoso A, Minutti CM, Pereira da Costa M, Reis e Sousa C, Sousa C. Dendritic cells revisited. *Annu Rev Immunol*. 2021;39(1):131-166.
22. Chen L, Flies DB. Molecular mechanisms of T cell co-stimulation and co-inhibition. *Nat Rev Immunol*. 2013;13(4):227-242.
23. Jenkins MK, Taylor PS, Norton SD, Urdahl KB. CD28 delivers a costimulatory signal involved in antigen-specific IL-2 production by human T cells. *J Immunol*. 1991;147(8):2461-2466.
24. Leitner J, Herndler-Brandstetter D, Zlabinger GJ, Grubeck-Loebenstein B, Steinberger P. CD58/CD2 is the primary costimulatory pathway in human CD28-CD8+ T cells. *J Immunol*. 2015;195(2):477-487.
25. Binder C, Cvetkovski F, Sellberg F, et al. CD2 immunobiology. *Front Immunol*. 2020;11:1090.
26. Bachmann MF, Barner M, Kopf M. Cd2 sets quantitative thresholds in T cell activation. *J Exp Med*. 1999;190(10):1383-1392.
27. Linsley PS, Ledbetter JA. The role of the CD28 receptor during T cell responses to antigen. *Annu Rev Immunol*. 1993;11:191-212.
28. Esensten JH, Helou YA, Chopra G, Weiss A, Bluestone JA. CD28 costimulation: from mechanism to therapy. *Immunity*. 2016;44(5):973-988.
29. Fraietta JA, Lacey SF, Orlando EJ, et al. Determinants of response and resistance to CD19 chimeric antigen receptor (CAR) T cell therapy of chronic lymphocytic leukemia. *Nat Med*. 2018;24(5):563-571.
30. Cohen AD, Garfall AL, Stadtmauer EA, et al. B cell maturation antigen–specific CAR T cells are clinically active in multiple myeloma. *J Clin Invest*. 2019;129(6):2210-2221.

31. Fritsch RD, Shen X, Sims GP, Hathcock KS, Hodes RJ, Lipsky PE. Stepwise differentiation of CD4 memory T cells defined by expression of CCR7 and CD27. *J Immunol*. 2005;175(10):6489-6497.

32. Martin MD, Badovinac VP. Defining memory CD8 T cell. *Front Immunol*. 2018;9:2692.

33. Gumber D, Wang LD. Improving CAR-T immunotherapy: overcoming the challenges of T cell exhaustion. *EBioMedicine*. 2022;77:103941.

34. Ross SH, Cantrell DA. Signaling and function of interleukin-2 in T lymphocytes. *Annu Rev Immunol*. 2018;36:411-433.

35. Guil-Luna S, Sedlik C, Piaggio E. Humanized mouse models to evaluate cancer immunotherapeutics. *Annu Rev Cancer Biol*. 2021;5(1):119-136.

36. Trobridge GD, Beard BC, Gooch C, et al. Efficient transduction of pigtailed macaque hematopoietic repopulating cells with HIV-based lentiviral vectors. *Blood*. 2008;111(12):5537-5543.

37. Taraseviciute A, Tkachev V, Ponce R, et al. Chimeric antigen receptor T cell-mediated neurotoxicity in nonhuman primates. *Cancer Discov*. 2018;8(6):750-763.

38. Nooij FJ, Jonker M, Balner H. Differentiation antigens on rhesus monkey lymphocytes. II. Characterization of RhT3, a CD3-like antigen on T cells. *Eur J Immunol*. 1986;16(8):981-984.

39. Buchholz CJ, Friedel T, Büning H. Surface-engineered viral vectors for selective and cell type-specific gene delivery. *Trends Biotechnol*. 2015;33(12):777-790.

40. Agarwal S, Hanauer JDS, Frank AM, Riechert V, Thalheimer FB, Buchholz CJ. In vivo generation of CAR T cells selectively in human CD4+ lymphocytes. *Mol Ther*. 2020;28(8):1783-1794.

41. Frank AM, Weidner T, Brynza J, Uckert W, Buchholz CJ, Hartmann J. CD8-specific designed ankyrin repeat proteins improve selective gene delivery into human and primate T lymphocytes. *Hum Gene Ther*. 2020;31(11-12):679-691.

42. Jamali A, Kapitza L, Schaser T, Johnston ICD, Buchholz CJ, Hartmann J. Highly efficient and selective CAR-gene transfer using CD4- and CD8-targeted lentiviral vectors. *Mol Ther Methods Clin Dev*. 2019;13:371-379.

43. Pfeiffer A, Thalheimer FB, Hartmann S, et al. In vivo generation of human CD19-CAR T cells results in B-cell depletion and signs of cytokine release syndrome. *EMBO Mol Med*. 2018;10(11):e9158.

44. Frank AM, Braun AH, Scheib L, et al. Combining T-cell-specific activation and in vivo gene delivery through CD3-targeted lentiviral vectors. *Blood Adv*. 2020;4(22):5702-5715.

45. Dobson CS, Reich AN, Gaglione S, et al. Antigen identification and high-throughput interaction mapping by reprogramming viral entry. *Nat Methods*. 2022;19(4):449-460.

46. Cunningham J, Chandra S, Emmanuel A, et al. In vivo delivery of a CD20 CAR using a CD8-targeted fusosome in Southern pig-tail macaques (M. nemestrina) results in B cell depletion [abstract]. *Blood*. 2021;138(suppl 1):2769.

47. Andorko JI, Russell RM, Schnepp BC, et al. Targeted in vivo generation of CAR T and NK cells utilizing an engineered lentiviral vector platform. *Blood*. 2023;142(suppl 1):763.

48. Amirache F, Lévy C, Costa C, et al. Mystery solved: VSV-G-LVs do not allow efficient gene transfer into unstimulated T cells, B cells, and HSCs because they lack the LDL receptor. *Blood*. 2014;123(9):1422-1424.

49. Pan D, Gunther R, Duan W, et al. Biodistribution and toxicity studies of VSVG-pseudotyped lentiviral vector after intravenous administration in mice with the observation of in vivo transduction of bone marrow. *Mol Ther*. 2002;6(1):19-29.

50. Pfeifer A, Kessler T, Yang M, et al. Transduction of liver cells by lentiviral vectors: analysis in living animals by fluorescence imaging. *Mol Ther*. 2001;3(3):319-322.